Photo-degradation of acid red 44 using Al and Fe modified silicates

Medhat Mohamed El-Moselhy*

Chemistry Department, Faculty of Science, Al-Azhar University, Nasr City, Cairo, Egypt

ARTICLE INFO

ABSTRACT

Al and Fe modified silicates were synthesized using the hydrothermal method. The obtained materials were calcined at different temperatures (250, 500 and 750 °C) and characterized using XRD, FTIR, UV and SEM spectroscopy. The obtained materials were applied for the photo-decolorization of acid red 44 as a member of azo dye family, in aqueous medium using UV irradiation ($\lambda = 254$ nm) under different experimental conditions. The effect of calcination temperature, catalyst concentration and pH on the decolorization of acid red 44 dye were investigated. The decolorization of acid red 44 dye and the decreasing in concentration of the formed intermediates have been followed using UV–vis spectrophotometry and high performance liquid chromatography (HPLC). Results showed that the addition of Al and Fe-silicate to the dye solution as well as pH change greatly enhanced the rate of degradation. The decolorization followed the pseudo first order kinetics model and a significant mineralization of AR44 was observed.

© 2009 Elsevier B.V. All rights reserved.

1. Introduction

Pigments, dyes and their derivatives are used in many industries such as paints, textile, leather, paper, pharmaceutical, cosmotics, etc. Wastewater discharged from textile industries has different characteristics from those of other industries. Dyes discharged through textile wastewater give high colors that inhibit light penetration, and many synthetic dyes do not easily decompose in biological treatments due to their toxic effects on microorganisms. Azo dyes constitute a major part of all commercial dyes [1,2]. Several derivatives of azo dyes are known to presrent serious carcinogenic effect [3]. It has been reported that in a typical process approximately 10% of the dye is lost during dyeing processes and is released into wastewater [4]. Removal of such colored materials from wastewater to meet the environmental regulations exhust a great part from economic income. In recent years the human need for water increases due to the limitted sources of water, for this reason the treatment of wastewater have attracted the attention of many researchers. Recycling and reuse of wastewater is a necessity nowadays due to the dwindling amount of water available for human use.

Advanced oxidation process (AOP) have been developed and extensively used for non-destructive physical water treatment processes, such as adsorption on the surface of certain substances. Heterogeneous photocatalysis represents an example of AOP capable of achieving a complete oxidation of organic and inorganic species, including dyes. But this method may lead to another secondary pollution and require further treatment. Oxidation of colored material using photo energy in combination with catalysts constitute a promising attractive technique for the treatment processes. The combination of semiconductor material such as metal oxides (TiO_2, ZnO and Fe_2O_3) and metal sulfides (CdS and ZnS) as photocatalysts for the degradation of organic contaminants have been extensively used [5–17].

Due to its large specific surface area and suitable chemical properties to support catalytic reactions, metal silicates are used extensively as adsorbent for large number of aqueous contaminants [18–27]. In particular, silica supported iron-based catalysts have attracted much research attention due to their use in the Fisher Tropsh process. This type of materials supported on silica possess more efficient catalytic performances [18], for example high attrition resistance and excellent stability imparted by silica as backbone. However, the presence of silica also suppresses the reducibility and the activity of catalyst due to the variations in surface structure and interaction between iron and silica [17].

In the present work, we have described the synthesis of Al and Fe-modified silicates calcined at different tempratures and investigated the catalytic activity of the synthesized catalysts at different conditions (pH, initial concentration of pollutant and catalysts) in the photo-decolorization of acid red 44 dye as a model compound as a representative of anionic dye of acid class.

2. Experimental methods

2.1. Chemicals

Disulfonic azo dye [AR44] (98% purity) with the molecular formula showed in Table 1 is used as a substrate. $Al_2(SO_4)_3$, $FeCl_3$

* Tel.: +20 106292802; fax: +20 222630677.
  E-mail address: medhatmohamed@yahoo.com.

Na-silicate were purchased from Fluka, AR grade were used as received without further purification.

2.2. Synthesis

For the synthesis of silica modified catalyst [16,18], a solution of sodium silicate was added into Fe chloride and Al sulfate solutions. The reaction mixtures were kept under constant stirring and heating at 100 °C for about 2 h in an autoclave. After that the resulting solution was filtered to separate the precipitates. The filtered cake was consequently dried at 100 °C overnight and calcined at 250, 500 and 700 °C for 5 h. The metal cation (Fe and Al) thus prepared to silica ratios were found to be 2:1 for Fe and Al-silicate for the materials (denoted as Al-silicate and Fe-silicate), respectively. The materials were characterized by various techniques such as X-ray diffraction (XRD), ultraviolet–visible (UV–vis) spectroscopy, scanning electron micrscopy (SEM), FTIR and low temperature N_2 adsorption measurements.

2.2.1. Catalyst characterization
2.2.1.1. Experimental techniques.
The X-ray diffractograms of various zeolites samples were measured by using a Bruker axs, D8 advance diffractometer (Billerica, USA). The patterns were run with Ni-filtered copper radiation ($\lambda = 1.54$ Å) at 30 kV and 10 m A with a scanning speed of $2\theta = 2.5°$ min^{-1}.

The FT-IR spectra were recorded on a Bruker (Vector 22, USA), single beam spectrometer with a resolution of 2 cm$^{(1}$. The samples (20 mg/cm^2) were ground with KBr as a tablet and mounted to cavity of the instrument while flushing with nitrogen gas.

The nitrogen adsorption isotherms were measured at −196 °C using a conventional volumetric apparatus. The specific surface area was obtained using the BET method.
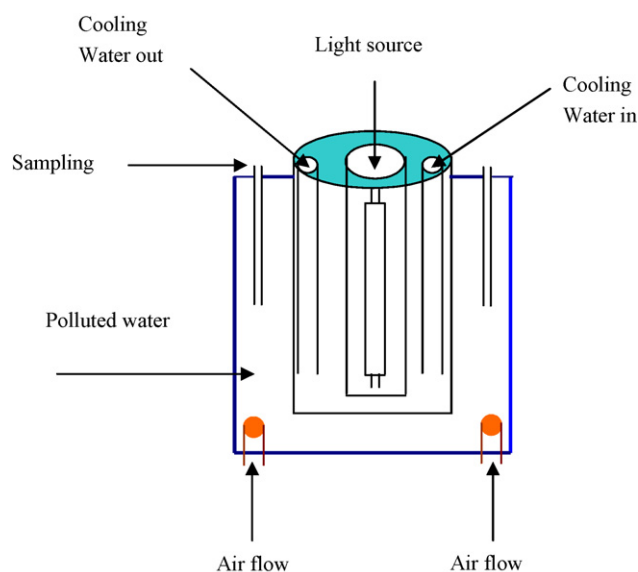
Scanning electron micrographs were obtained using a Joel scanning microscope model JSM5410 (Japan). Samples were deposited on a sample holder with an adhesive carbon foil and sputtered with gold.

2.2.2. High performance liquid chromatography (HPLC)
The degradation intermediates were analyzed by HPLC using at definite time intervals (Dionex p580 pump) equipped with Dionex 202 TP^{TM} C18 column (4.6 × 250 mm, USA) with eluent consisting of a 60:40 acetonitrile:water mixture under a flow rate of 1 ml/min. The degradation intermediates followed the decolorization of AR44 dye was detected by using UV-detector in the UV range (200–300).

2.2.3. Irradiation experiments
To 200 ml of dye solution, catalysts were added and the resulting suspension was subjected to UV irradiation by immersing 6 W Hg lamp (254 nm) within the photoreactor (Scheme 1) where a total radiant flux (20 MW cm^2) were applied. The radiation flux was measured by a UV radiometer (Digtal, UVX, 36). All measurements were performed at 25 °C. The aqueous suspension was magnetically stirred throughout the experiment. At different time intervals aliquot was withdrawn which was subsequently, filtered through 0.45 μm (Millipore) syringe filter. Absorption spectra were recorded and rate of decolorization was observed in terms of change in intensity at λ max of the dyes (518 nm). Similar experiments were carried out by varying the pH of the solution (pH 2–10), the ini-

Scheme 1. Simplified diagram of photoreactor used in our study.

tial concentration of dye (0.0001–0.1 M) and the catalyst loading (0.1–0.3 g/l).

3. Results and discussion

3.1.1. Structural properties

The structural properties of silica-free and silica-supported catalysts as-prepared were contrasted to illustrate the effect of aluminum and iron–silica interactions. The aluminum and iron phases in catalysts were identified by using XRD, IR and SEM spectroscopy. The XRD patterns of the catalyst samples as-synthesized are presented in Figs. 1 and 2. The patterns show that the silica-free catalyst exhibits amorphous structure as reported in literatures. The result also implies that iron phase in catalyst Fe–Si (Fig. 1) is well-crystallized as α-Fe$_2$O$_3$, which is almost identical with the reference pattern of hematite in terms of both line position as well as relative intensity. Furthermore, a new diffraction lines at $2\theta = 27.5, 32.5$ were found, which are assigned for the characteristic of Fe$_2$SiO$_4$ phase when compared with the instrument Fe-silicate standards. On the other hand the XRD patterns of aluminum (Fig. 2) shows the characteristics diffraction lines of crystalline Al-silicate as that of zeolites [12,17].

3.1.2. IR spectra of various samples

The FT-IR spectra of Fe–Si and Al–Si calcined at 773 K are shown in Fig. 3 in the range 450–1700 cm^{-1}. The IR spectrum of Fe-silicate shows bands at 1130, 1062, 937, 790, 612 and 458 cm$^{(1}$, which are assigned to different vibrations of tetrahedral and framework atoms in silicate structure [28–30]. The bands at about 1130 and 464 cm$^{(1}$ are due to internal vibrations of (Si, Al)O$_4$ tetrahedra of silicate structure, whereas the bands at about 1062, 790, and 612 cm$^{(1}$ are due to vibrations related to external linkages between tetrahedra and hence are sensitive to framework structure [31,32]. Further-

Table 1
Typical characteristics of dye used in this study.

Commercial name	Color index dye name	Molecular formula	Molecular weight (g/mol)	λ_{max} (nm)	C.I. number
Crystal scarlet	Acid red 44	$C_{20}H_{12}N_2Na_2O_7S_2$	502.43	518	16250

Fig. 1. XRD patterns of calcined Fe-silicate in comparison with the parent Na-silicate.
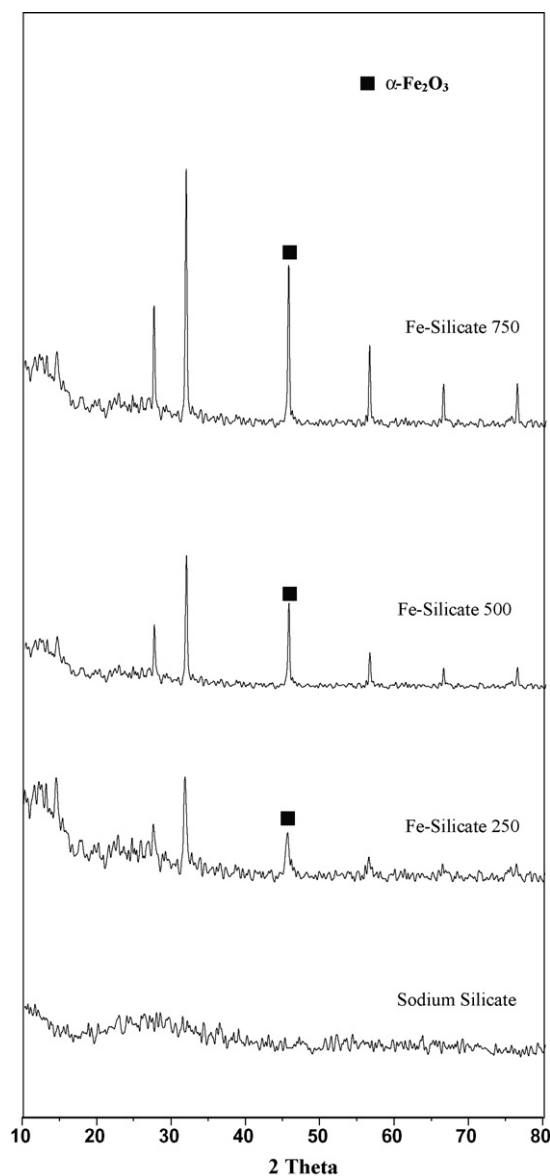

Fig. 2. XRD patterns of calcined Al-silicate in comparison with the parent Na-silicate.

more, the appearance of a new absorption band at 937 cm$^{(1}$ may be related to stretching vibrations of Fe–O bond.

3.1.2.1. IR spectra of hydroxyl region

Fig. 4 shows the FT-IR spectra of Al and Fe-silicate in the hydroxyl region. The Al–Si sample exhibits five bands at 3736, 3695, 3628, 3598 and 3520 (shoulder) cm^{-1}, similar to what is observed in most zeolite structures. The bands at 3736 and 3695 cm^{-1} are due to isolated silanol groups and hydroxyl groups attached to silica–alumina containing species, respectively. The structural acidic bridging Al–OH–Si groups (Brönsted acid sites) exhibit two peaks at 3628 and 3598 cm^{-1}, as observed in the case of other high-silica, large-pore zeolites such as mordenite [33,34] and ZSM-12 [35]. These peaks are assigned to bridging hydroxyl groups vibrating in the main 12-ring channels and in small six- or eight-membered ring channels [33,34], respectively.

The FT-IR spectrum of Fe–Si (Fig. 4) exhibits bands at 3738, 3700 (sh), 3650 (broad), 3615 and 3520 (broad) cm^{-1}. These bands are assigned to similar vibrations as for Al-silicate. However, due to the larger size and higher electronegativity of Fe compared to Al, the Fe–O bond lengths are larger than that of Al–O. This will cause
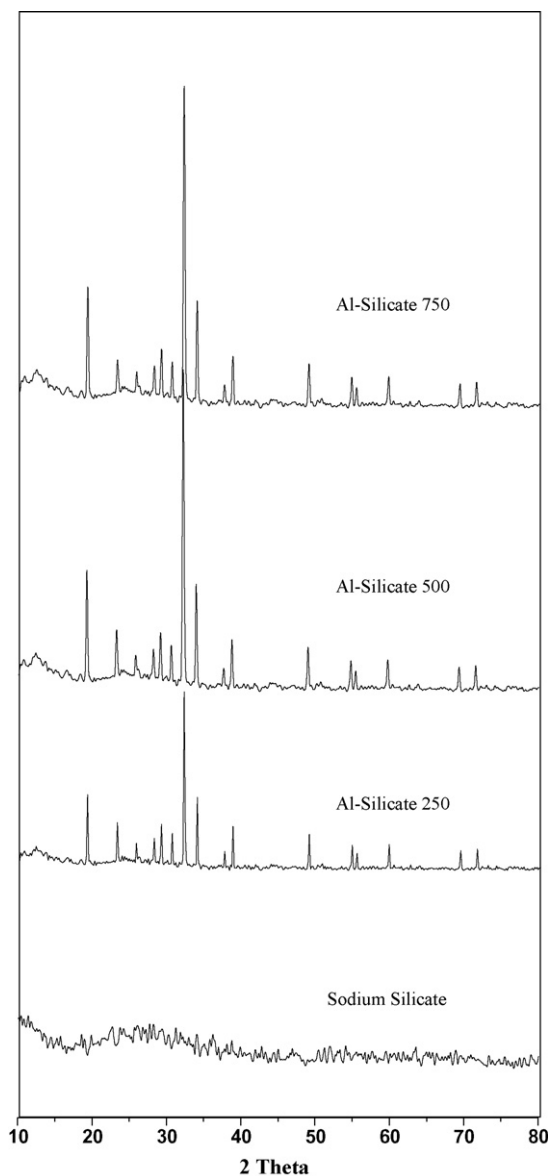
the bands Fe(OH)Si (3650 and 3615 cm^{-1}) to shift to higher wave numbers as compared to the Al(OH)Si (3628 and 3598 cm^{-1}) bands.

3.1.3. SEM

The influence of amorphous substitution on the morphology of the calcined Fe–Si and Al–Si materials was studied by SEM. Incorporation of heteroatom to amorphous structure as in silicate may lead to the increasing of crystallinity. The SEM pictures of the synthesized Al and Fe-silicates samples in comparison with the parent silicate are presented in Fig. 5. All pictures show non-homogeneous particle size distribution. The presence of elongated crystallites, with varying sizes could clearly be discerned for Hematite species form upon the calcination of Fe–Si (Fig. 5a and b). On the other hand, the aspect ratio of the crystallites seems to increase in case of Al–Si (Fig. 5c and d).

3.2. UV–vis

The UV–vis spectra of synthesized Fe and Al-silicates are shown in Fig. 6. the spectra show characteristic absorption bands around
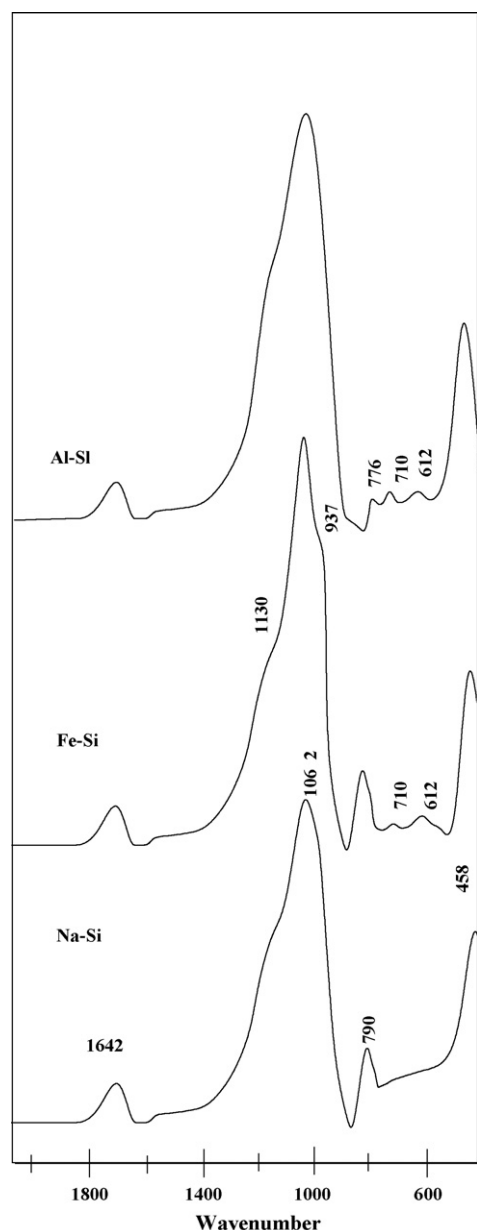
Fig. 3. FTIR Spectrum of the as synthesized Fe and Al-silicate in comparison with Na-silicate.

Fig. 4. FTIR Spectrum of the as synthesized Fe and Al-silicate in comparison with Na-silicate calcined at 777 K in the hydroxyl region.

256, 265, 275, 333 and 360 nm; the intensities of these bands vary upon the temperature at which they were calcined (250–750 °C). The appearance of these new bands upon modification with Fe species with increasing intensities (Fig. 6a) after calcination at 250, 500 and 750 °C calcination temperature, may be associated with ligand to metal charge transfer (CT) that involves isolated four co-coordinated Fe(III) and has been assigned to $t_1 \rightarrow e$ involving Fe(III) in [FeO$_4$] tetrahedral [29]. Furthermore, the spectrum of calcined Fe-silicate shows a small CT absorption band around 283 nm, which is assigned to Fe(III) species in octahedral coordination [30]. The appearance of this species indicates leaching of Fe(III) from the framework during calcination of the synthesized Fe-silicates.

On the other hand, the UV–vis spectra of Al-silicate (Fig. 6b) exhibits only one absorption band at 335 nm, same as that exist in the Fe-silicate. The appearance of this band may be assigned for Si–O–M bond in the five membered ring characterizing for zeolite structure.
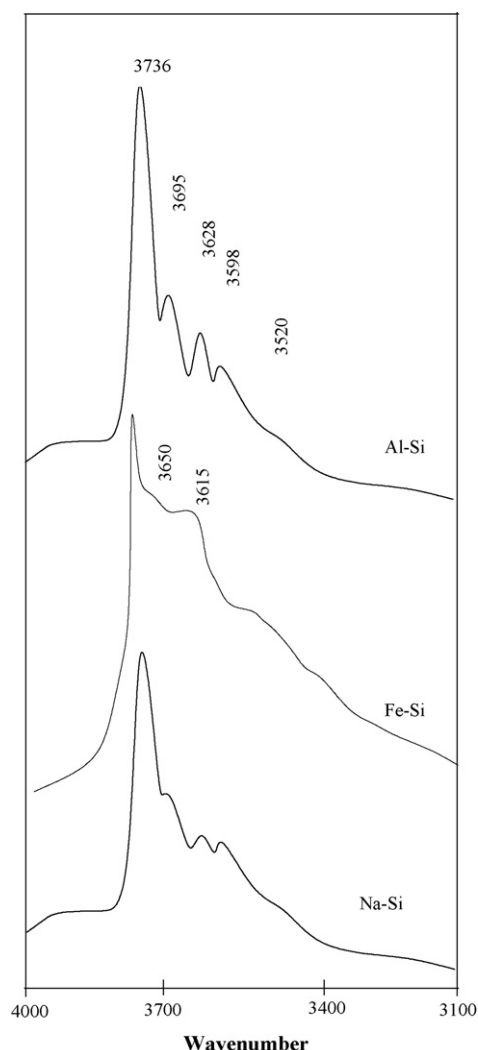
Generally, the appearance of some absorption bands in the range from 350 to 430 nm may indicate the formation of minute oxide species formed during calcination of the materials [31].

3.3. Surface area

The Nitrogen adsorption–desorption measurements indicate that the values of surface area increases with modification of silicate with Al and Fe cations and the obtained values are depicted in Table 2. The data also indicate that modification with Fe exhibits the largest surface area when compared with that modified with Al cations.

3.4. Catalytic activity

3.4.1. Adsorption of AR44 on Fe and Al-silicates

Since the rate of reaction for most catalytic processes generally depends on the amount of adsorbed molecules which then start to mineralize upon exposure to UV irradiation, a series of experiments were carried out in the dark to study the adsorption of AR44 dye on Fe and Al-silicates surface that calcined at different calcination temperature (250, 500 and 750 °C). It was found that an
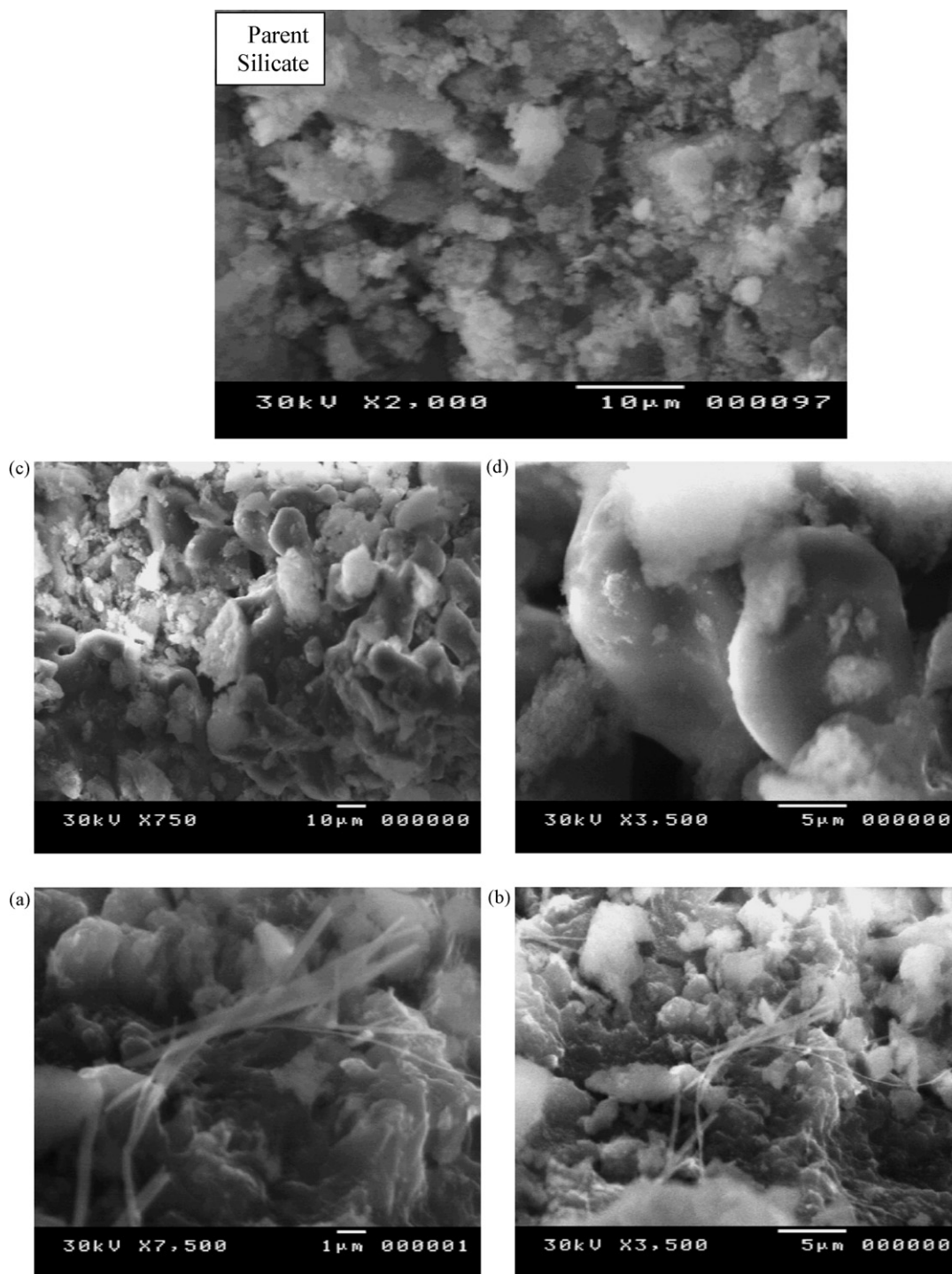
Fig. 5. SEM pictures of synthesized (a, b) Fe-silicate and (c, d) Al-silicate in comparison with the parent Na-silicate.

equilibrium adsorption of a Langmuir type was reached in less than 30 min.

According to the Langmuir model the coverage θ varies as

$$\theta = \frac{Q_{ads}}{Q_{max}} = \frac{KC_{eq}}{1 + KC_{eq}} \tag{1}$$

where Q_{ads} is the number of adsorbed molecules at the adsorption equilibrium, Q_{max} the maximal adsorbable quantity, K the Langmuir adsorption constant of AR44 on Fe and Al-silicates and C_{eq} the concentration of AR44 at the adsorption equilibrium.

The data plotted in Fig. 7 represents the linear transformation of Eq. (1) which is expressed by the following equation:

$$\frac{1}{Q_{ads}} = \frac{1}{Q_{max}} + \frac{1}{Q_{max}KC_{eq}} \tag{2}$$

In this curve, the ordinate at the origin is equal to the reciprocal of Q_{max}, whereas K can be calculated from the slope (slope = $1/Q_{max}K$).

In Table 3, adsorption parameters for AR44 were reported; it appears that the value of K is in agreement with that of other dyes which have an analogous structure [35].
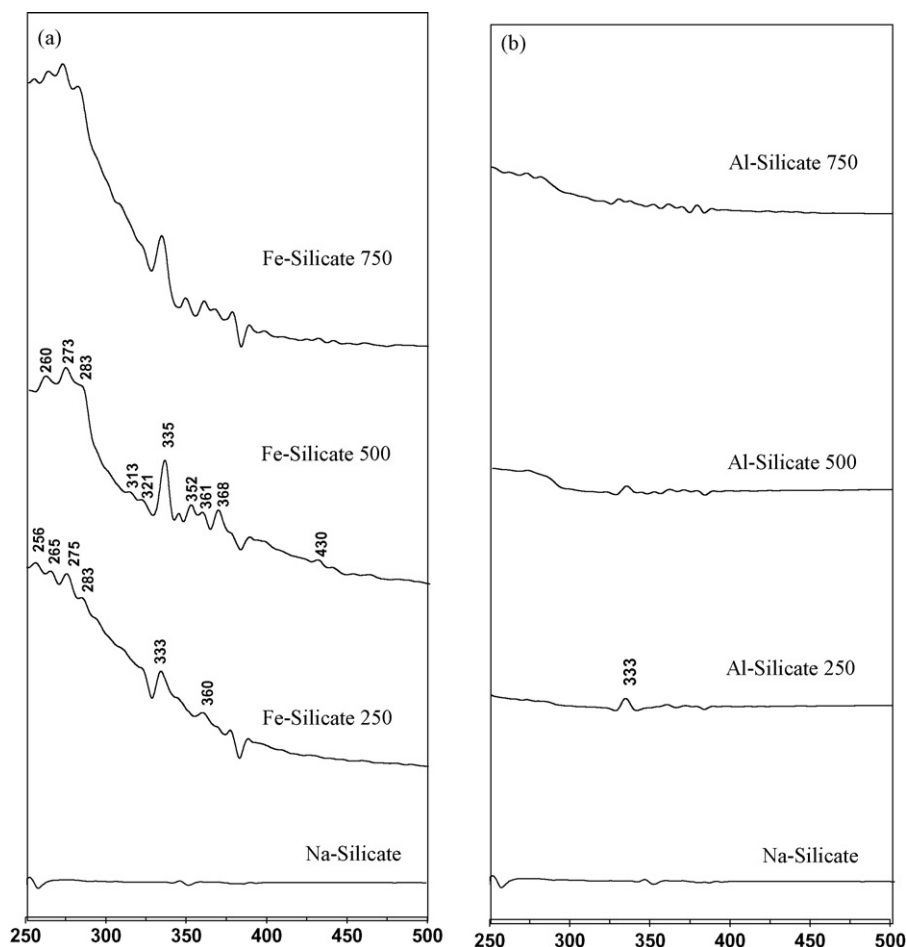
Fig. 6. UV–vis spectra of synthesized and calcined: (a) Fe-silicate, (b) Al-silicate.

3.4.2. Removal of AR44

Acid red 44 dye is one of the azo dye family having sulphonate (SO_3^-) and azo groups showing absorption peaks at 518 and 338 nm. The photo-decolorization experiments were carried out under UV light. The efficiency of decolorization was observed for different doses of Fe and Al-silicate catalysts. The rate of decolorization was recorded in terms of change in intensity of characteristic peaks.

3.4.3. UV–vis spectra of dyes

Fig. 8 shows typical time dependent UV–vis spectrum of AR44 during photoirradiation. AR44 shows absorption peaks at 518 and 338 nm in visible and UV region respectively. The rate of decolorization was recorded with respect to the change in intensity of absorption peaks at 518 and 338 nm. The absorption peaks, corresponding to dyes diminished and finally disappeared during reaction, which indicated that the dyes had been degraded.

3.4.4. Decolorization of AR44 dye using Fe and Al-silicates catalysts

Investigations were carried out with two different cation modified silicate in order to select the most effective catalyst for

Table 2
N$_2$ sorption results of Al and Fe modified Silicates.

Sample	BET surface area (m^2/g)
SiO$_2$	643
Al-silicate	850
Fe-silicate	1240

degradation of AR44 dye. Initially control experiments in the absence of catalyst either in dark or under light irradiation revealed neither the occurrence of decolorization nor any mineralization of AR44.

The photo-degradation experiments were carried out using different catalysts, various pH values (2, 4, 8 and 10) at fixed dye concentration (0.01 M) respectively. The results indicated that Fe-silicate exhibits higher photocatalytic activity than Al-silicate (Fig. 8). The greater efficiency of Fe-silicate over Al-silicate may be attributed to the formation of stable complex [AR44*···Fe^{3+}], between the adsorbed dye molecules and surface iron species, which absorbs the UV light and effectively produces AR44*$^{•+}$, Fe^{3+} (that later turns to Fe^{2+}) and organics which on further oxidation may lead to its successive degradation. Furthermore, Fe-silicate may have greater quantum efficiency than Al-silicate.

3.4.5. Effect of catalyst concentration

In order to determine the effect of catalyst dose, the experiments were performed by varying catalyst concentration from 0.1 to 0.3 g/l for dye solutions of 0.1 M at natural pH 6.0. The decolorization efficiency for various catalysts dose for Fe and Al-silicates has been depicted in Fig. 9a and b. The data obtained reveals that initial slopes of the curves increase greatly by increasing catalyst dose from 0.1 to 0.3 g/l for Fe and Al-silicate. In case of Fe-silicate maximum decolorization is observed with 0.3 g/l calcined at 750 °C after 6 min degradation time whereas, for Al-silicate it was possible to decolorize the dye as small as 0.3 g/l dose of catalyst calcined at 750 °C. However, in this case irradiation time was more than 15 min. This can be explained on the basis that the increase of catalyst
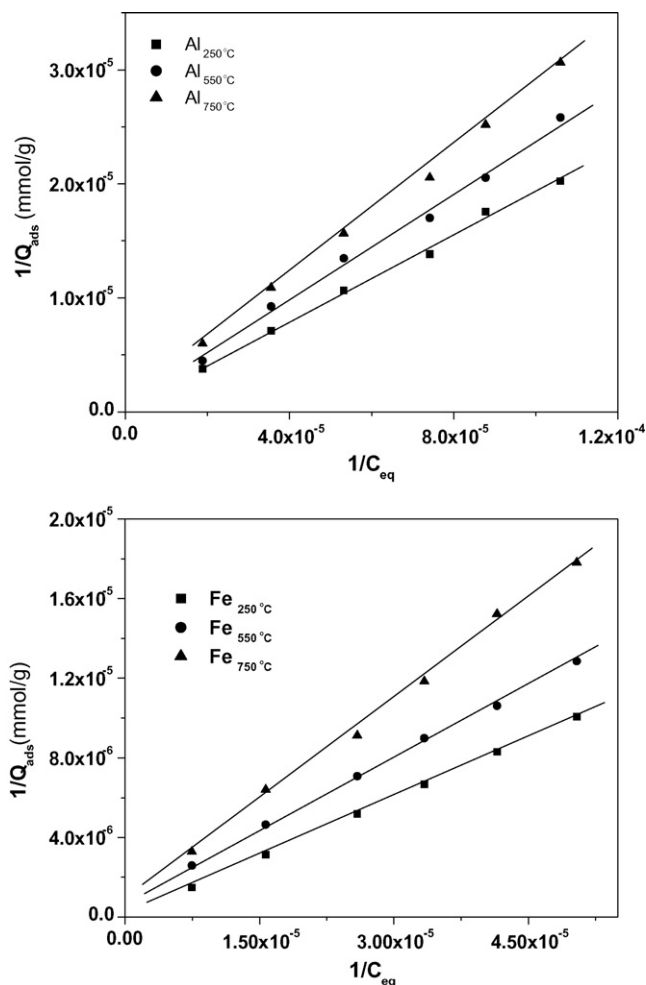
Fig. 7. Transformation of Langmuir isotherm: reciprocal of the quantity adsorbed as a function of reciprocal of equilibrium concentration at different calcination temperature of the catalysts.

dosage as well as calcination temperature, total active surface area increases; hence availability of more active sites on catalyst surface also increases [36–40]. At the same time, due to an increase in turbidity of the suspension with high dose of photocatalyst, there will be decrease in penetration of UV light and hence photoactivated
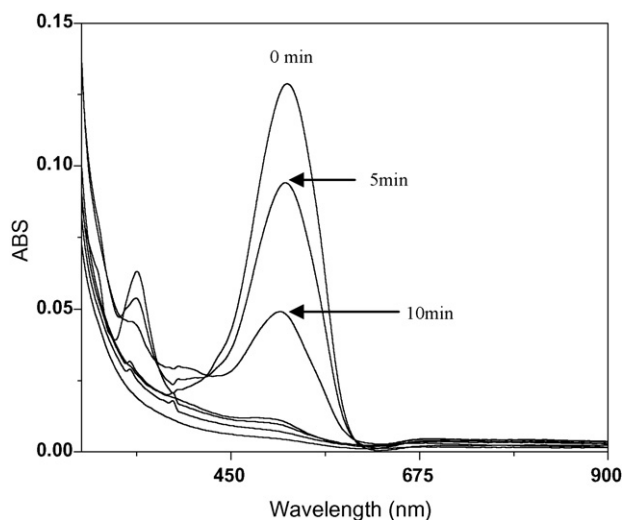

Fig. 8. Absorbance spectra of AR44 dye during the decolorization using Fe-silicate.

Table 3
Adsorption parameters for AR44.

Sample	Al-silicate			Fe-silicate		
Calcination temperature (°C)	250	500	750	250	500	750
Q_{max}	43.3	52.6	45.4	52.6	64.2	49.4
K ($l\,mol^{-1}$)		941			1330	

volume of suspension decreases [33]. Thus it can be concluded that higher dose of catalyst may not be useful both in view of aggregation as well as reduced irradiation field due to light scattering.

3.4.6. Effect of pH

Wastewater containing dyes is discharged at different pH; therefore it is important to study the role of pH on decolorization of dye. To study the effect of pH on the decolorization efficiency, experiments were carried out at various pH values, ranging from 2 to 10 at a constant dye concentration (0.01 M) and catalyst dose (0.1 g/l), respectively, for AR44 dye. Fig. 10 shows the color removal efficiency of AR44 dye as a function of pH. It has been observed that the decolorization efficiency decreases with increase in pH exhibiting maximum rate of degradation at pH 4 for Fe-silicate and pH 6 for Al-silicate. Similar behavior has also been reported for the photocatalytic decolorization of azo dyes [31,32,34]. The interpretation of pH effects on the efficiency of the photocatalytic decolorization process is not straight forward because of its multiple roles. First, it is related to the acid base property of the metal silicate surface and can be explained on the basis of zero point charge. The adsorption of water molecules at surficial metal sites is followed by the dissociation of OH^- charge groups leading to coverage with chemically equivalent metal hydroxyl groups (M–OH) [40]. Due to amphoteric behavior of most metal hydroxides, the following two equilibrium reactions are considered [Eqs. (3) and (4)]

$$M\text{–}OH + H^+ \rightarrow M\text{–}OH_2^+ \qquad (3)$$

$$M\text{–}OH \rightarrow M\text{–}O^- + H^+ \qquad (4)$$

The zero point charge (zpc) for Fe-silicate is 6.05 ± 0.3. Therefore, Fe-silicate surface is positively charged below pH 6 and above this pH, surface is negatively charged. The presence of large quantities of OH^- ions on the particle surface as well as in the reaction medium favors the formation of $OH^\bullet$ radical, which is widely accepted as principal oxidizing species responsible for decolorization process at acidic pH level and results in enhancement of the efficiency of the process [32].

The experimental results revealed that higher degradation of the dyes occurred in acidic region than in case of basic region. For Fe-silicate, rate of photodecolorization decreased with increase in pH, exhibiting maximum efficiency (100%) at pH 4 after 6 min from the start of irradiation, beyond which the rate of degradation remained constant. This may be attributed to the electrostatic interactions between the positive catalyst surface and dye anions leading to strong adsorption of the latter on the metal oxide support. On the other hand, in case of Al-silicate 100% decolorization was observed at pH values of 2%, 4%, 6% and 80% decolorization was observed at pH 10 after 20 min from the start of irradiation (Table 3).

3.4.7. Kinetic study

Optimization of the catalyst oxidation behavior is necessary to apply any process economically viable. In all experiments with Fe and Al–Si system, the decolorization is observed to follow a pseudo first order reaction kinetics with respect to AR44 (Eq. (5))
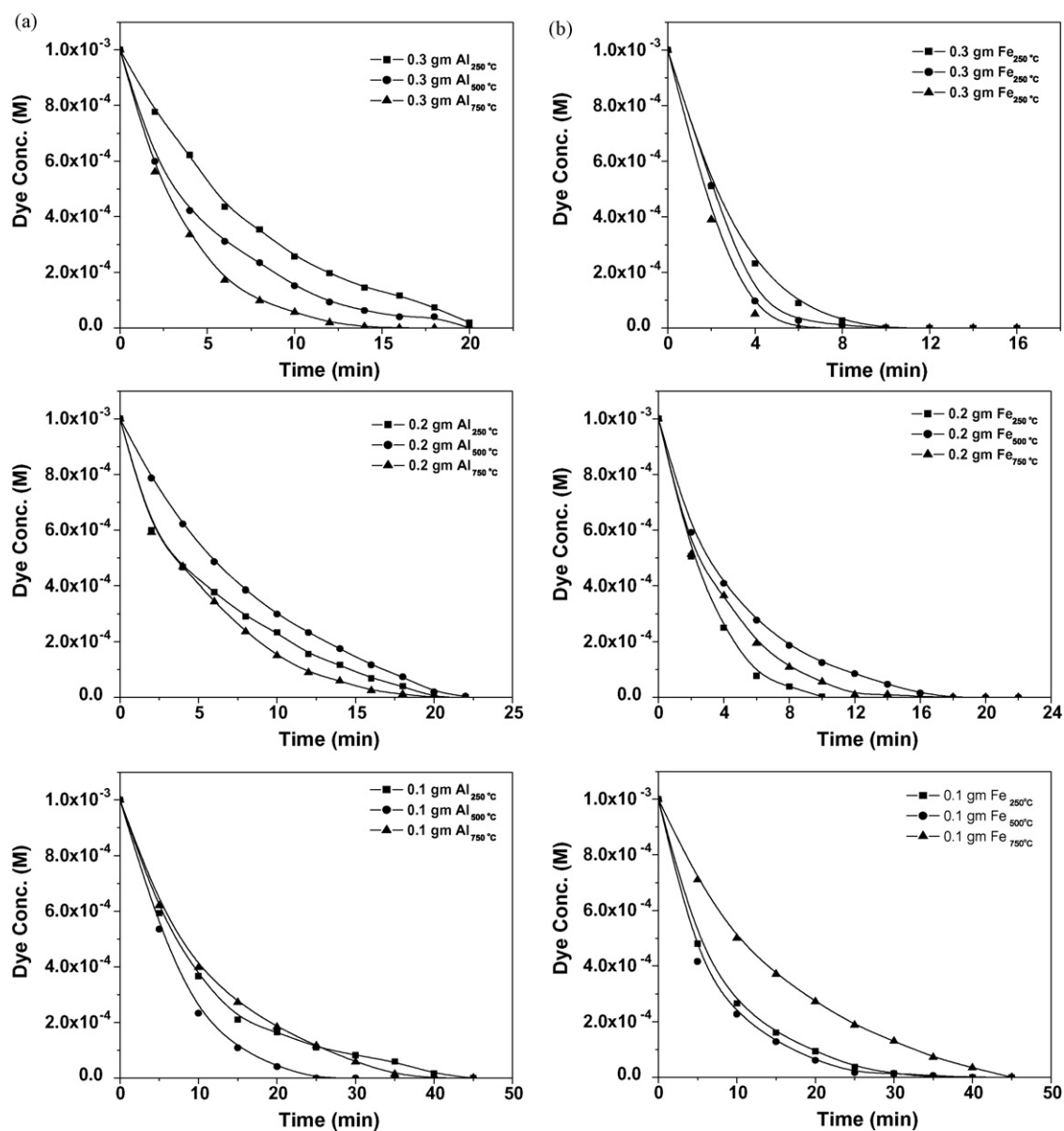
$$\ln\left(\frac{C_t}{C_o}\right) = kt \qquad (5)$$

Fig. 9. Variation of degradation rate with time for the photodegradation of AR44 in aqueous solutions on (a) Fe-silicates (b) Al-silicates.
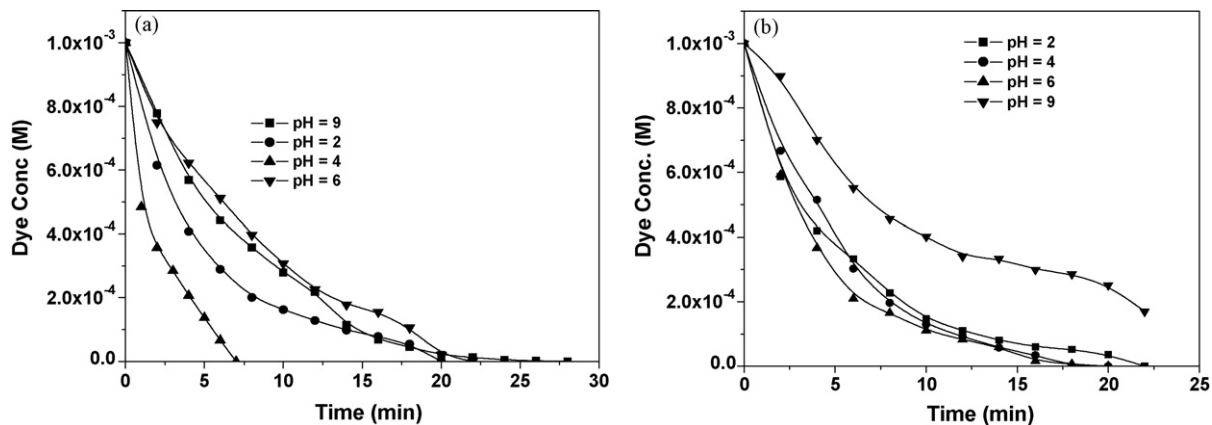

Fig. 10. Effect of pH change on the degradation rate for the photodegradation of AR44 in aqueous on (a) Fe-silicates (b) Al-silicates.
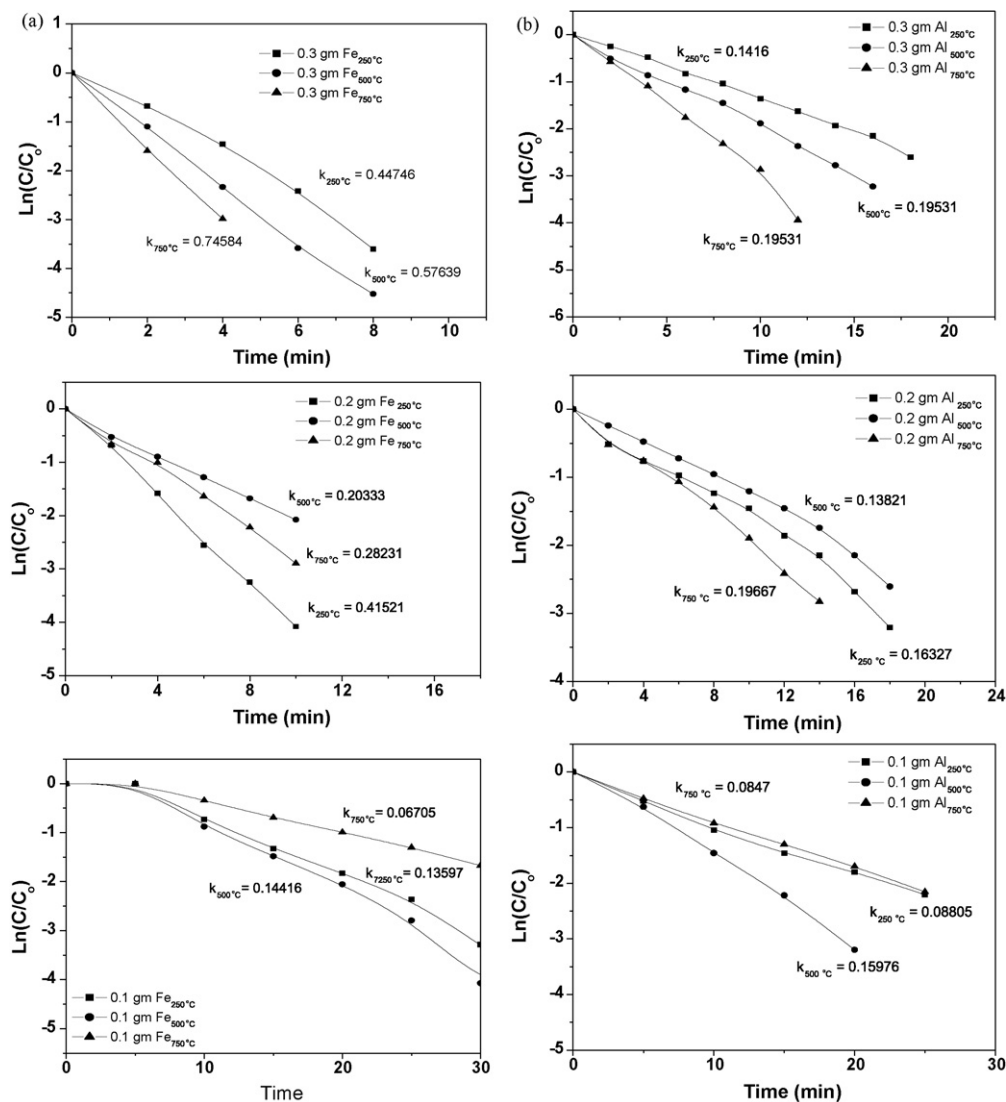
Fig. 11. Apparent first order linear transformation $\ln(C/C_o) = f(t)$ for the photodegradation of AR44 in aqueous solutions on. (a) Fe-silicates (b) Al-silicates.

where C_o and C_t refer the initial concentration and the concentration at any time t of the dye and k is the pseudo-first order rate constant. A straight lines passing through the origin were observed when ln (C_t/C_o) values were plotted against t conforming the assumed first order kinetics as shown in Fig. 11a and b. The slope of the plots produced the pseudo-first order rate constant (k) show the kinetics of disappearance of AR44 dye for an initial concentration of 0.01 M under optimized conditions. The results show that the semi-logarithmic plots of the concentration data gave a straight line and the correlation constants for the fitted line were depicted in Table 4.

3.4.8. Mineralization investigations

Due to the probability of higher toxicity of formed intermediates followed the process of organic compounds degradation, mineralization of the compound should be ensured before discharging the treated waste water into the ecosystem. The mineralization of AR44 degradation intermediates were followed up by HPLC analysis. The data indicates the formation of both acetic and formic acids as intermediates (Fig. 12) followed the process of degradation. The efficiency of cation modified silicates would be obtained by comparing the concentration values observed for the dye degradation and mineralization in both Fe-silicate and Al-silicate systems. The plot

Table 4
Values of calculated K_{ap} for the photodegradation of AR44 dye Using Al and Fe-silicates.

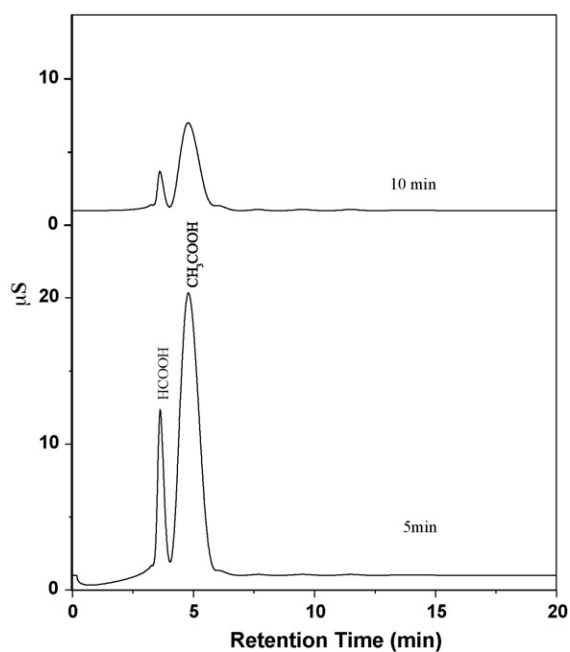| Sample	Catalyst dose	K_{ap} for different temprature calcined catalysts		
		250 °C	500 °C	750 °C
Al-silicate	0.1	0.0881	0.1597	0.0847
	0.2	0.163	0.138	0.197
	0.3	0.142	0.195	0.315
Fe-silicate	0.1	0.136	0.144	0.067
	0.2	0.415	0.282	0.203
	0.3	0.447	0.576	0.746

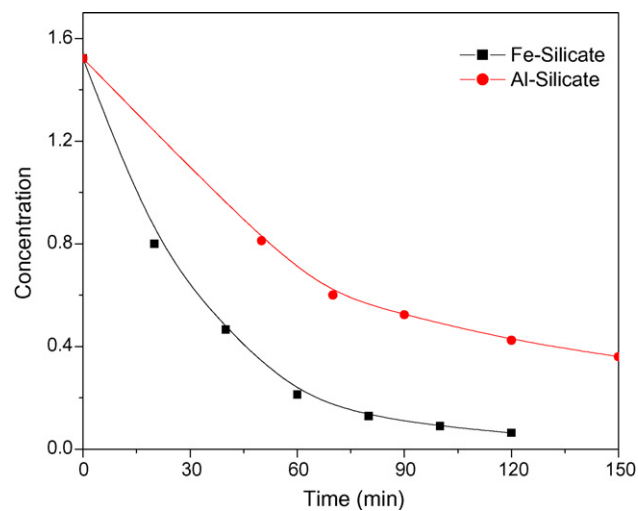**Fig. 12.** HPLC chromatogram of the detected degradation intermediates.

Fig. 13. Mineralization of AR44 dye (reaction conditions: pH 4; 0.3 g Fe and Al-silicate).
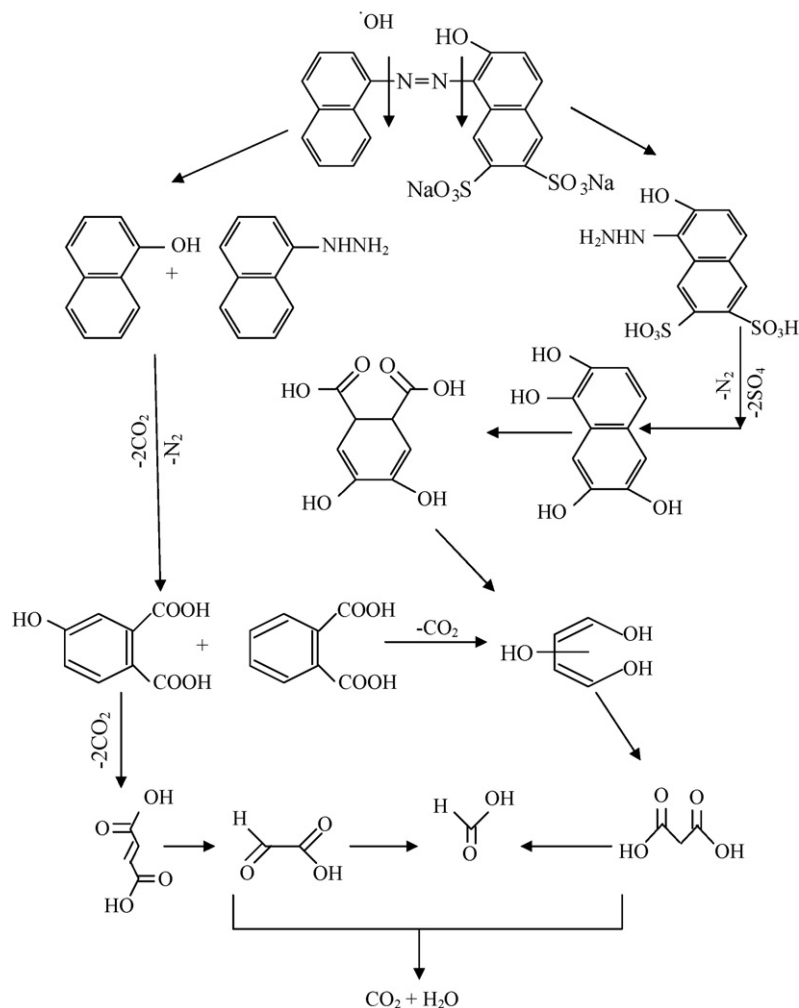

Fig. 14. Proposed mechanism for the photocatalytic degradation pathways of acid red 44.

of intermediate concentration against irradiation time is presented in Fig. 13. The obtained data reveal that the decrease in intermediate concentration after 125 min of irradiation is 76.36% in the case of Al-silicate whereas it is 95.7% when Fe-silicate is used. Thus, HPLC confirms the efficiency of Fe over Al-silicate for the photodegradation of the AR44. Fig. 14 illustrates the proposed mechanism and the expected pathway for the degradation intermediates of AR44 dye.

4. Conclusions

Experimental investigation in this study has demonstrated that the AR44 can be degraded by UV irradiation in the presence of Fe and Al-silicate as a catalyst. Adsorption plays an important role in the degradability of the dye. By examining the key factors including pH values, Fe and Al-silicate concentration, it is clear that the effect of Fe and Al-silicates concentration as well as variation of calcination temperature of the catalysts greatly enhance the rate of decolorization and beneficially raise the first-order kinetic constant. By comparing results, it is concluded that Fe-silicate is most active in the removal of AR44 dye at our experimental conditions (calcined at 500 °C and pH 4).

Acknowledgments

References

[1] M.A. Behnajady, n. Modirshahla, N. Daneshver, M. Rabbani, J. Hazard. Mater. 140 (2007) 257–263.
[2] k. Golka, S. Kopps, Z.W. Myslak, Toxicol. Lett. 151 (2004) 203.
[3] L. Young, J. Yu, Water Res. 31 (1997) 1187.
[4] M. Stylidi, D.I. Kondarides, X.E. Verkios, Appl. Catal. B 40 (2003) 271.
[5] M. Karkmaz, E. Puzenat, C. Guillard, J.M. Hermann, Appl. Catal. B 51 (2004) 183–194.
[6] M. Perez-Urquiza, J.L. Beltran, J. Chromatogr. A 898 (2000) 271.
[7] M.A. Behnajady, N. Modirshahla, M. Shokri, Chemosphere 55 (2004) 129.
[8] N. Daneshvar, D. Salari, M.A. Behnajady, Iran. J. Chem. Eng. 21 (2002) 55–62.
[9] M.A. Fox, M.T. Dulay, Chem. Rev. 93 (1993) 341.
[10] (a) D.F. Ollis, E. Pelizzetti, N. Serpone, Environ. Sci. Technol. 25 (1991) 1523;
(b) N. Serpone, Res. Chem. Int. 20 (1994) 953.
[11] (a) A. Mills, S. Le Hunte, J. Photochem. Photobiol. A 108 (1997) 1;
(b) H. Al-Ekabi, N. Serpone, J. Phys. Chem. 92 (1988) 5726.
[12] P.V. Kamat, Chem. Rev. 93 (1993) 267.
[13] M.R. Hoffmann, S.T. Martin, W. Choi, D.W. Bahnemann, Chem. Rev. 95 (1995) 69.
[14] H. Hidaka, S. Horikoshi, K. Ajiaka, J. Zhao, N. Serpone, J. Photochem. Photobiol. A 108 (1997) 197.
[15] H. Hidaka, J. Zhao, E. Pelizzetti, N. Serpone, J. Phys. Chem. 96 (1992) 2226.
[16] M.M. El-Moselhy, M.M. Emara, A.S. Turky, Eg. J. Chem. 49 (2) (2006) 241–259.
[17] M.M. Emara, M.M. El-Moselhy, A.S. Turky, J. Hazard. Mater., in press, doi:10.1016/j.jhazmat.2008.11.044.
[18] M.M. Mohamed, J. Colloid Interface Sci. 272 (2004) 28–34.
[19] M.A. Brown, S.C. De Vito, Crit. Rev. Environ. Sci. Technol. 23 (1993) 249.
[20] H. Lachheb, E. Puzenat, A. Houas, M. Ksibi, E. Elaloui, C. Guillard, J.-M. Herrmann, Appl. Catal. 39 (2002) 75.
[21] S.H. Lin, C.F. Peng, Water Res. 30 (1996) 587.
[22] H.A. Al-Ekabi, D. Ollis, Photocatalytic Purification and Treatment of Water and Air, Elsevier, Amsterdam, 1993.
[23] O. Legrini, E. Oliveros, A.M. Braun, Chem. Rev. 93 (1993) 671.
[24] X.S. Zhao, Q. Ma, G.Q. Lu, Energy Fuels 12 (1998) 1051.
[25] H. Yoshida, A. Okamoto, T. Kataoka, Chem. Eng. Sci. 48 (1993) 2267.
[26] M.M. Mohamed, I. Mekkawy, J. Phys. Chem. Solids 64 (2003) 299.
[27] X. Hu, S. Qiao, X.S. Zhao, G.G. Lu, Ind. Eng. Chem. Res. 40 (2001) 862.
[28] H. Gies, Z. Kristallogr. 175 (1986) 93.
[29] T. Brar, P. France, P.G. Smimiotis, Ind. Eng. Chem. Res. 40 (2001) 1133.
[30] S. Bordiga, R. Buzzoni, F. Geobaldo, C. Lamberti, E. Giamello, A. Zecchina, G. Leofanti, G. Petrini, G. Tozzola, J. Catal. 158 (1996) 486.
[31] S. Bordiga, R. Buzzoni, F. Geobaldo, C. Lamberti, E. Giamello, A. Zecchina, G. Petrini, G. Tozzola, J. Catal. 158 (1999) 187.
[32] M.M. Mohamed, I. Othman, N.A. Eissa, Microporous Mesoporous Mater. 87 (2005) 93.
[33] J.C. Jansen, F.J. van der Gaag, H. van Bekkum, Zeolites (1984) 369.
[34] P.A. Jacobs, H.K. Beyer, J. Valyon, Zeolites 1 (1981) 161.
[35] H. Laccheb, E. Puzenat, A. Houas, M. Kasibi, E. Alaloui, C. Guillard, J.M. Hermann, Appl. Catal. B: Environ. 39 (2002) 75–80.
[36] C. Lizama, J. Freer, J. Baeza, H.D. Mansilla, Optimized photodegradation of reactive blue 19 on TiO₂ and ZnO suspensions, Catal. Today 76 (2002) 235.
[37] A. Akyol, H.C. Yatmaz, M. Bayramoglu, Photocatalytic decolorization of remazol red RR in aqueous ZnO suspensions, Appl. Catal. B: Environ. 54 (2004) 19.
[38] N. Daneshvar, D. Salari, A.R. Khataee, Photocatalytic degradation of azo dye acid red 14 in water on ZnO as an alternative catalyst to TiO₂, J. Photochem. Photobiol. A: Chem. 157 (2003) 111.
[39] S. Sakthivel, B. Neppolian, B.V. Shankar, B. Arabindoo, M. Palanichamy, V. Murugesan, Solar photocatalytic degradation of azo dye: comparison of photocatalytic efficiency of ZnO and TiO₂, Sol. Energy Mater. Sol. Cells 77 (2003) 68.
[40] M.S.T. Gonclaves, A.M.F. Oliveira-Campose, E.M.M.S. Pinto, P.M.S. Plasencia, M.J.R.P. Queiroz, Photochemical treatment of solutions of azo dyes containing TiO₂, Chemosphere 39 (1999) 781.